Please do not adjust margins

Journal Name

ARTICLE

3D Bragg coherent diffractive imaging of five-fold multiply twinned gold nanoparticle

Received 00th January 20xx,
Accepted 00th January 20xx

DOI: 10.1039/x0xx00000x

www.rsc.org/

Jong Woo Kim[a,b†], Andrew Ulvestad[a,c], Sohini Manna[d], Ross Harder [b], Eric E. Fullerton[d], and Oleg. G. Shpyrko[a]

The formation mechanism of five-fold multiply twinned nanoparticles has been a long-term topic because of their geometrical incompatibility. So, various models have been proposed to explain how the internal structure of the multiply twinned nanoparticle accommodates the constraints of the solid-angle deficiency. We investigate the internal structure, strain field and strain energy density of a 600 nm sized five-fold multiply twinned gold nanoparticle quantitatively using Bragg coherent diffractive imaging, which is suitable for the study of buried defects and three-dimensional strain distribution with great precision. Our study reveals that the strain energy density in a five-fold multiply twinned gold nanoparticle is an order of magnitude higher than the single nanocrystals such as an octahedron and triangular plate synthesized under the same conditions. This result indicates that the strain developed while accommodating angular misfit, although partially released through the introduction of structural defects, is still large throughout the crystal.

Introduction

The structural investigation of the five-fold multiply twinned nanoparticles has been an attractive research topic within the materials science community because of not only their beneficial properties [1-3], but also the geometrical incompatibility, the five-fold decahedrons are packed completely by the tetrahedral subunits despite angular lattice misfit. Understanding the detailed structures and inherent strain fields in these nanoparticles are crucial to understanding the stabilization of the structure and growth mechanism, and ultimately to tailoring their unique properties. Accordingly, decahedral particles and five-fold twinning, which is the most common form for multiple cyclic twinning [4], have been studied considerably through both experiment and theory [5-14]. The observation of the internal structure has been performed using a wide range of techniques such as aberration-corrected high-resolution electron microscopy (HREM) [15-18], transmission electron microscopy (TEM) [19] and high-resolution high-angle annular dark field (HAADF) scanning transmission electron microscopy (STEM) [20-21]. Not only experimental techniques, but also the simulations based on finite elementary method (FEM) [22, 23] and molecular dynamics (MD) [24,25] have been conducted to study the internal structure and/or strain of the five-fold multiply twinned nanoparticles. These techniques are not directly sensitive to the three-dimensional (3D) strain distribution inside the nanocrystal, which is an essential characteristic to understand the packing mechanism with solid-angle deficiency. Here, we use Bragg coherent x-ray diffractive imaging (Bragg CDI) to study the morphology, lattice distortion, and strain energy density within an individual multiply twinned nanocrystal. This imaging technique is suitable for the study of buried defects and three-dimensional strain distribution with great precision [26-28].

In a Bragg CDI measurement, a sample is placed in the focused x-ray beam and aligned appropriately so that the Bragg condition is satisfied and the Bragg peak appears on the detector in the far field. To acquire the 3D diffraction intensity, the sample needs to be rocked within a small angular range and the collected 2D slices of diffraction intensity are stacked together. As a result of phase retrieval [29, 30], we can obtain the Bragg electron density (i.e. the shape of the nanocrystal) and the displacement field with subangstrom resolution, in full 3D detail for the sample. If there is any portion of the sample not satisfying the Bragg condition, it is invisible in the reconstructed Bragg electron density [31]. The retrieved phase is interpreted as the displacement along the direction of momentum transfer vector and a value of 2π phase is equivalent to a displacement of one d-spacing of the Bragg reflection plane. In addition, the strain distribution can be obtained by taking derivatives in the appropriate directions of the displacement field.

[a] *Department of Physics, University of California-San Diego, La Jolla, California 92093-0319, USA*
[b] *Advanced Photon Source, Argonne National Laboratory, Argonne, Illinois 60439, USA.*
[c] *Materials Science Division, Argonne National Laboratory, Argonne, Illinois 60439, USA.*
[d] *Center for Magnetic Recording Research, University of California-San Diego, La Jolla, California 92093-0401, USA*
† *E-mail: jw.kim@anl.gov*

Please do not adjust margins

Please do not adjust margins

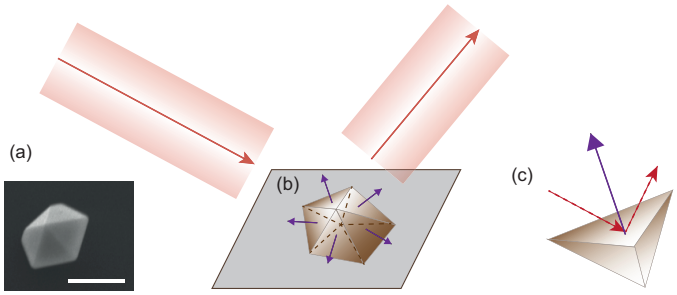

Figure 1: (a) SEM image of five-fold multiply twinned nanoparticle. The white scale bar represents 600 nm. (b) Schematic of experimental configuration showing the illumination of x-ray beam on the sample and a diffractive x-ray beam going out to the detector. The normal directions of crystalline planes (111) are marked by the purple arrows. (c) One of subunits can satisfy the Bragg condition while others do not.

Experiments

Bragg CDI experiment

The Bragg CDI measurements were performed at Sector 34-ID-C of the Advanced Photon Source (APS) synchrotron facility. An upstream monochromator was used to select E = 9.0 KeV x-rays, which were focused onto the sample using Kirkpatrick-Baez mirrors that focused the beam to a 2µm x 2µm region. The resulting diffraction patterns were measured using a charge-coupled device (CCD) with 22.5 µm pixels located along the detector arm at a distance of 0.9 m beyond the sample. In this experiment, we reconstruct both the 3D distribution of Bragg electron density ρ (x, y, z) with 17 nm spatial resolution and the 3D lattice displacement field projected along (111), u_{111} (x, y, z), and consequently, we obtain the 3D strain distribution of the nanoparticle along the momentum transfer direction, Q_{111}, by derivative of the displacement field.

Preparation of samples

Au nanocrystals were grown using thermal chemical vapor deposition (CVD) onto a Si (100) substrate with the native oxide using a catalyst-free thermal approach with $AuCl_3$ as a precursor [32]. Approximately 1.0 g of powdered $AuCl_3$ was loaded in a boat and placed within a quartz tube at the center of a Lindberg Blue furnace at 475°c. An Ar carrier gas was flowed through the quartz tubing while the downstream end of the CVD setup remained isolated from the outside atmosphere. The system was left at 475 °c for about an hour, after which it was allowed to cool down to room temperature. The Ar flow through the quartz tube was maintained for the duration of the cooling process.

Results and Discussion

The morphology of the five-fold gold nanoparticle is shown in the scanning electron microscope (SEM) in Fig.1 (a). The nanoparticles created by this synthesis method is useful to study the intrinsic strain [33] because this method produces highly pure nanoparticles without using any external surfactants, capping layers, or stabilizers, which might be attached on the final product and affect the strain on the surface. This approach yields various shape of gold nanoparticles, such as octahedrons, triangular plates, icosahedrons, and five-fold multiply twinned particles.

The five-fold multiply twinned nanoparticles consist of tetrahedral subunits, that is, equally shaped subunits are joined to the neighboring tetrahedron by twin boundaries. Each subunit has a (111) crystallographic facet and they point to the different outward directions as shown in Fig. 1(b). For this reason, even if the x-ray beam illuminates the entire sample, just one of subunits can satisfy the Bragg condition as shown in Fig. 1(c) and thereby, one of subunits can be recovered via the phase retrieval algorithm.

Fig. 2(a) shows the reconstructed Bragg electron density as a green isosurface. It has an edge length of 360 nm and a height of 270 nm. In comparison with the SEM image, the reconstructed image shows half of the tetrahedral subunit. This is due to the fact that the other half subunit has its own (111) crystallographic face. So, there are 10 segments that have their own (111) crystallographic facets in a five-fold decahedral gold nanoparticle and we measured a half of a subunit. Some void regions are observed in the reconstructed Bragg electron density. This absence of the electron density is indicative of the presence of the region that does not satisfy the Bragg condition. These absent volumes look like a patch adjacent to a twin boundary, a small tetrahedron parallel to the other twin boundary, and an irregular shape at a grain boundary shared with the other half of subunit.

If the five-fold decahedron is enclosed by perfect face-centered cubic (fcc) tetrahedral subunits, a solid-angle deficiency of 7.35° remains [16, 34]. This solid-angle deficiency could be accommodated by a homogeneous strain, that is, a structural change from face-centered cubic (fcc) to a body-centered orthorhombic (bco) structure [35-37] or the introduction of a single wedge disclination that coincides with the five-fold axis of the nanoparticle, which is so-called inhomogeneous strain model. The latter model produces an inhomogeneous strain field that reduces the total strain energy [38-40].

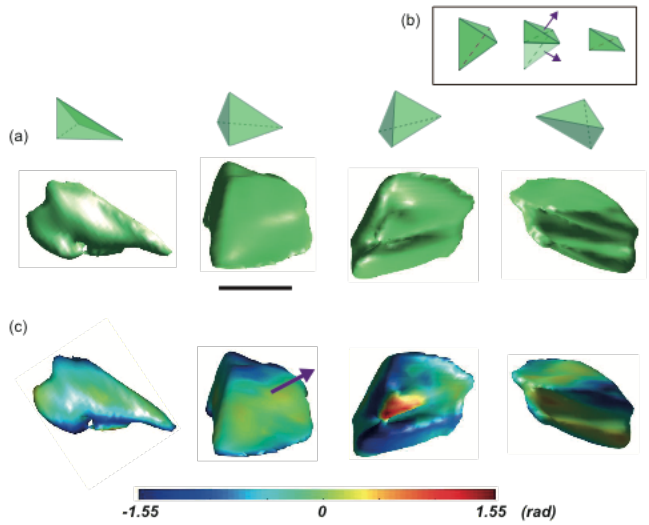

Figure 2: (a) Isosurface rendering of the Bragg electron density representing the particle shape from four different viewing angles with guiding models such as one twin boundary, (111) facet plane, bottom surface, and the other twin boundary, respectively. The scale bar represents 300 nm. (b) A model of regular tetrahedral subunit that can be divided by an upper and a lower part with different (111) facets, implying that the Bragg electron density is a half subunit. (b) The local value of the phases at the surface represented by the color. The phase is projected onto momentum transfer vector (111), which is normal to the facet.

This journal is © The Royal Society of Chemistry 20xx

Please do not adjust margins

Please do not adjust margins

This solid-angle deficiency generates defects inside of the subunits and impose the strain at the twin boundaries [16]. The dislocations usually occur to relieve elastic strain energy in the particles with a size of hundreds of nanometers [16]. The stacking faults and dislocations can be identified based on the Bragg electron density and displacement field. It is known that the stacking fault can lead to voids in the Bragg electronic density [41, 42] and that edge and screw dislocations generate particular displacement fields [43, 44]. Thus, the absence of the Bragg electron density can be attributed to presence of stacking fault. According to the previous studies [15, 45, 46], the stacking faults were observed adjacent to a twin boundary, on which the shear strain is concentrated. The stacking faults look like a small tetrahedron, which is parallel to one of twin boundaries, and were also observed in five-fold multiply twinned nanoparticle [15, 18, 47]. Our observation of missing Bragg electron density is consistent with the previous studies in term of the stacking fault locations. Thus, we conclude that the stacking faults are responsible for invisible Bragg electron density. Fig. 2 (c) shows a displacement distribution projected onto (111) direction, which is indicated by a purple arrow, on the surface of a half tetrahedral subunit. A maximum value of 1.55 *rad*, for example, represents that the unit cells in this location are deformed from their equilibrium lattice spacing between (111) planes by 1.0 Å.

Figure. 3 (a) shows the strain distribution on the surface of the particle, which is obtained by the derivative of the displacement field, ranging from -0.46 % to 0.20 %. This result is comparable to the strain range ±0.54 % measured by Johnson *et al*. [16]. Recall that the decahedron was created with many different shapes of gold nanocrystals at the same time. The magnitude of the strain is higher than the single nanocrystals such as the octahedron (±0.05 %) and the triangular plate (±0.06 %) [33] that were synthesized through the same process. However, it is much less than 2%, which is calculated from solid-angle deficiency (i.e. $7.35^{o} \div 360^{o}$). Therefore, the strain is released through the generation of structural defects so it is lower than the strain under the assumption of perfect tetrahedral subunits enclosed, which results in the solid-angle deficiency. But the strain level of multiply twinned gold nanoparticle is still higher than the single crystals.

Figure. 3 (b) and (c) show three vertical and horizontal slice planes, respectively. The strain magnitude around stacking faults, which is adjacent to the twin boundary and parallel to the twin boundary is relatively low, but the strain is concentrated on the grain boundary shared with the other half subunit. The average of the strain magnitude over each slice is plotted as shown in Fig. 3 (d) and (e). The averaged strain magnitude is fairly constant in most of the vertical slices except for both sides, where the twin boundaries are. However, the averaged strain over the horizontal slices decreases from the grain boundary surface with the highest value to the top vertex. This result indicates that the strains are relieved around the stacking faults adjacent and parallel to the twin boundaries, where the strain typically are concentrated [16, 18]. Instead, the strong strain remains around the buried defect in the middle of subunit. The locally concentrated strain in the grain boundary can be indicative of the fact that the grain boundary generates partial dislocations, requiring high stress [48].

We also evaluate the elastic strain energy E_s and the strain energy density (i.e. strain energy per volume) using the three-dimensional strain distribution.

$$E_s = \int \frac{1}{2}\Sigma_{ij}\sigma_{ij}\epsilon_{ij}dV = \frac{2G+3I}{2}\int\left(\frac{\partial u_{111}}{\partial x_{111}}\right)^2 dV \qquad (1)$$

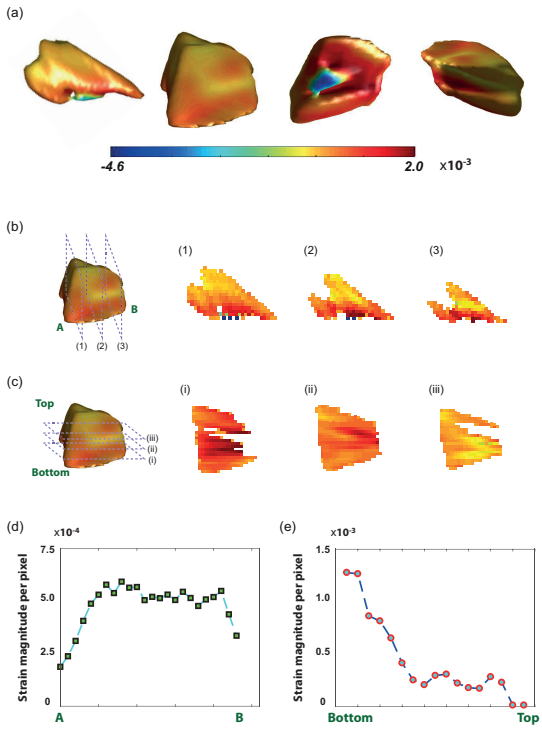

Figure 3: (a) The strain distribution on the surface. (b) & (c) Two-dimensional strain distributions in vertical and horizontal cross-sections, indicated by three dashed windows, respectively. (d) Plot of strain magnitude per pixel in vertical cross-sections from left A to right B in (b). (e) Plot of strain magnitude per pixel in horizontal cross-sections from the bottom to the top in (c).

where G and I are the Lame constants for the material and the volume integral is over the entire Bragg electron density, not the entire decahedron. A component of strain, which is projected on the momentum transfer vector (111), is used to evaluate the elastic strain energy. Because gold is a cubic lattice structure, it is sufficient to represent the strain energy over the volume [49]. It turns out that the strain energy density is 3.3×10^5 J/m^3. In this study, we calculated the elastic strain energy density for the octahedron and triangular plate that have been studied previously [33]. The octahedron with an edge length of 220nm and triangular plate with the thickness of 600nm and the height of 60nm have 7.6×10^4 J/m^3 and 4.0×10^4 J/m^3 for the strain energy density, respectively. As we observed above, introduction of structural defects may reduce the strain energy and sustain the stability of the nanostructure, which usually occurs in large (>100nm) sized five-fold twinned nanoparticle. However, it does not relieve the strain to the level of single nanoparticles because the magnitude of the elastic strain energy density is an order higher than the single nanocrystals (Table 1).

	Decahedron	Octahedron	Triangular plate
Strain Energy Density (J/m^3)	3.3×10^5	7.6×10^4	4.0×10^4

Table 1: The elastic energy density of multiply twinned nanoparticle (decahedron) and single nanoparticles (octahedron and triangular plate).

Please do not adjust margins

Please do not adjust margins

Conclusions

In conclusion, we have carried out a Bragg coherent diffractive imaging of a 600 nm sized five-fold twinned gold nanoparticle to investigate the details of internal structure and strain energy density. A quantitative study of real-space structure inversion reveals that there are defects such as stacking faults in the subunit of multiply twinned nanoparticle. They are present as a patch adjacent to a twin boundary and a small tetrahedron in the bulk of tetrahedral subunits, parallel to a twin boundary, and irregular shape at the grain boundary. In addition, the strain energy density is an order of magnitude higher than the single nanoparticles such as the octahedron and the triangular plate synthesized under the same circumstances. Our study shows that the structural defects are responsible for the strain relief and stabilization of the structure, but the strain still remains in the multiply twinned gold nanoparticle. In future work, it is necessary to obtain the reconstruction of the entire nanoparticle by combinations of each subunit for better understanding of the overall structure and the interaction between each subunit.

Acknowledgements

The coherent x-ray imaging work at UCSD was supported by US Department of Energy, Office of Science, Office of Basic Energy Sciences, under Contract DE-SC0001805. Crystal growth was supported by NSF DMR-1411335. Use of the Advanced Photon Source, an Office of Science User Facility operated for the U.S. Department of Energy (DOE) Office of Science by Argonne National Laboratory, was supported by the U.S. D.O.E. under Contract No. DE-AC02-06CH11357.

References

1. M. J. Walsh, K. Yoshida, A. Kuwabara, M. L. Pay, P. L. Gai, and E. D. Boyes, On the structural origin of the catalytic properties of inherently strained ultrasmall decahedral gold nanoparticles. Nano Lett. 2012, 12, 2027−2031.

2. A. M. Leach, M. McDowell, and K. Gall, Deformation of top-down and bottom-up silver nanowires. Adv. Funct. Mater. 2007, 17, 43−53.

3. D. Seo, C. I. Yoo, I. S. Chung, S. M. Park, S. Ryu, and H. Song, Shape adjustment between multiply twinned and single-crystalline polyhedral gold nanocrystals: Decahedra, Icosahedra, and Truncated Tetrahedra. J. Phys. Chem. C 2008, 112, 2469−2475.

4. H. Hofmeister, Forty years study of fivefold twinned structures in small particles and thin films. Cryst. Res. Technol. 1998, 33, 3−25.

5. A. I. Kirkland, P. P. Edwards, D. A. Jefferson, and D. G. Duff, The structure, characterization, and evolution of colloidal metals. Annu. Rep. Prog. Chem. C, 1990, 87, 247–304.

6. M. Jose-Yacaman, and M. Avalos-Borja, Electron-microscopy of metallic nanoparticles using high-resolution and medium-resolution techniques. Catal. Rev.-Sci. Eng. 1992, 34, 55–127.

7. V. G. Gryaznov, J. Heydenreich, A. M. Kaprelov, S. A. Nepijko, A. E. Romanov, and J. Urban, Pentagonal symmetry and disclinations in small particles. Cryst. Res. Technol. 1999, 34, 1091–1119.

8. L. D. Marks, Inhomogeneous strains in small particles. Surf. Sci. 1985, 150, 302–318.

9. L. D. Marks and D. J. Smith, High resolution studies of small particles of gold and silver: I. Multiply-twinned particles J. Cryst. Growth, 1981, 54, 425–432.

10. L. D. Marks, Modified wulff constructions for twinned particles J. Cryst. Growth, 1983, 61, 556–566.

11. L. D. Marks, Surface-structure and energetics of multiply twinned particles Phil. Mag. A, 1984, 49, 81–93.

12. L. D. Marks, Experimental studies of small-particle structures Rep. Prog. Phys. 1994, 57, 603–649.

13. L. M. Dorogin, S. Vlassov, A. L. Kolesnikova, I. Kink, R. Lohmus and A. E. Romanov, Crystal mismatched layers in pentagonal nanorods and nanoparticles Phys. Status Solidi B,2010, 247, 288–298.

14. M. Dorogin, S. Vlassov, A. L. Kolesnikova, I. Kink, R. Lohmus and A. E. Romanov, Pentagonal nanorods and nanoparticles with mismatched shell layers J. Nanosci. Nanotechnol. 2010, 10, 6136–6143.

15. H. Hofmeister, Lattice defects in decahedral multiply twinned particles of palladium. Z. Phys. D, 1991, 19, 307-310.

16. C. L. Johnson, E. Snoeck, M. Ezcurdia, B. Rodríguez-González, I. Pastoriza-Santos, L.M. Liz-Marzán, and M. J. Hÿtch, Effects of elastic anisotropy on strain distributions in decahedral gold nanoparticles. Nat. Mater., 2008, 7, 120-124.

17. W.H. Ji, W. H. Qi, X. Li, S. L. Zhao, S. S. Tang, H. C. Peng and S. Q. Li, Investigation of disclinations in marks decahedral Pd nanoparticles by aberration-corrected HRTEM Mater. Lett. 2015, 152, 283–286.

18. R. Yu, H. Wu, J. D. Wang, and J. Zhu, Strain concentration at the boundaries in 5-Fold twins of diamond and silicon. Appl. Mater. Interfaces, 2017, 9, 4253−4258.

19. C. C. Chen, C. Zhu, E. R. White, C. Y. Chiu, M. C. Scott, B. C. Regan, L. D. Marks, Y. Huang, and J. W. Miao, Three-dimensional imaging of dislocations in a nanoparticle at atomic resolution. Nature 2013, 496, 7443.

20. Goris, B., Beenhouwer, J. De., Backer, A. De., Zanaga, D., Batenburg, K. J., Sanches-Iglesia, A., Liz-Marzan, L. M., Aert, S. V., Bals, S., Sijbers, J., and Tendeloo, G. V. Measuring lattice strain in three dimensions through electron microscopy. Nano Lett., 2015, 15, 6996–7001.

21. L. D. Marks and D. J. Smith, HREM and STEM of defects in multiply-twinned particles J. Microsc. Oxford,1983, 130, 249–261.

 This journal is © The Royal Society of Chemistry 20xx

Please do not adjust margins

Please do not adjust margins

22. S. Patala, L. D. Marks, and M. Olvera de la Cruz, Elastic strain energy effects in faceted decahedral nanoparticles. J. Phys. Chem. C, 2013, 114, 1485–1494.

23. S. Patala, L. D. Marks, and M. Olvera de la Cruz, Thermodynamic analysis of multiply twinned particles: surface stress effects J. Phys. Chem. Lett., 2013, 4, 3089-3094.

24. Z. Zhang, S. Huang, L. Chen, Z. Zhu, and D. Guo, Formation mechanism of five-fold deformation twins in a face-centered cubic alloy. Sci. Rep., 2017, 7, 45405.

25. A. J. Cao, and Y. G. Wei, Formation of fivefold deformation twins in nanocrystalline face-centered-cubic copper based on molecular dynamics simulations. Appl. Phys. Lett., 2006, 89, 041919.

26. I. Robinson, and R. Harder, Coherent x-ray diffraction imaging of strain at the nanoscale. Nat. Mater. 2009, 8 (4), 291−298.

27. F. Hofmann, E. Tarleton, R. Harder, N. W. Phillips, P.-W. Ma, J. N. Clark, I. K. Robinson, B. Abbey, W. Liu, and C. E. Beck, 3D lattice distortions and defect structures in ion-implanted nano-crystals. Scientific Reports, 2017, *7*, 45993.

28. Y.-C. Chen-Wiegart, R. Harder, D. C. Dunand, and I. Mcnulty, Evolution of dealloying induced strain in nanoporous gold crystals Nanoscale, 2017, 9 (17) 5686-5693.

29. M. A. Pfeifer, G. J. Williams, I. A. Vartanyants, R. Harder, and I. K. Robinson, Three-dimensional mapping of a deformation inside a nanocrystal. Nature 2006, 442 (7098), 63−66.

30. M. C. Newton, S. J. Leake, R. Harder, and I. K. Robinson, Three-dimensional imaging of strain in a single ZnO nanorod, Nat. Mater., 2010, **9**, 120–124.

31. A. Ulvestad, J. N. Clark, R. Harder, I. K. Robinson, and O. G. Shpyrko, 3D imaging of twin domain defects in gold nanoparticles. Nano Lett. 2015, 15 (6), 4066−4070.

32. S. Manna, J. W. Kim, Y. Takahashi, O. G. Shpyrko, and E. E. Fullerton, Synthesis of single-crystalline anisotropic gold nano-crystals via chemical vapor deposition J. Appl. Phys., 2016, 119, 174301.

33. J. W. Kim, S. Manna, S. H. Dietze, A. Ulvestad, R. Harder, E. Fohtung, E. E. Fullerton, and O. G. Shpyrko, Curvature-induced and thermal strain in polyhedral gold nanocrystals Appl. Phys. Lett. 2014, 105, 173108.

34. T. K. Sau, and A. L. Rogach, Nonspherical noble metal nanoparticles: colloid-chemical synthesis and morphology control. Adv. Mater. 2010, 22, 1781–1804.

35. B. G. Bagley, A Dense packing of hard spheres with 5-fold symmetry. Nature 1965, 208, 674−675.

36. C. Y. Yang, Crystallography of decahedral and icosahedral particles: I. geometry of twinning. J. Cryst. Growth 1979, 47, 274−282.

37. S. Ino, Stability of multiply-twinned particles J. Phys. Soc. Japan 1969, 27, 941-953.

38. R. D. Wit, Partial Disclinations. J. Phys. C: Solid State Phys. 1972, 5, 529−534.

39. L. D. Marks, and A. Howie, Multiply-twinned particles in silver catalysts. Nature 1979, 282, 196−198.

40. Howie, A., and Marks, L.D. Elastic strains and the energy balance for multiply twinned particles. Philos. Mag. A, 1984, 49, 95

41. V. Favre-Nicolin, F. Mastropietro, J. Eymery, D. Camacho, Y. M. Niquet, B. M. Borg, M. E. Messing, L. –E. Wernersson, R. E. Algra, and E. P A M. Bakkers, T. H. Metzger, R. Harder, and I. K. Robinson, Analysis of strain and stacking faults in single nanowires using Bragg coherent diffraction imaging. New J. Phys. 2010, 12, 035013.

42. J. N. Clark, L. Beitra, G. Xiong, D. M. Fritz, H. T. Lemke, D. Zhu, M. Chollet, G. J. Williams, M. M. Messerschmidt, B. Abbey, R. Harder, A. M. Korsunsky, J. S. Wark, D. A. Reis, and I. K. Robinson, Imaging transient melting of a nanocrystal using an x-ray laser. Proc. Natl. Acad. Sci. U. S. A. 2015, 112, 7444−7448.

43. D. Hull, D. J. Bacon, Introduction to Dislocations (Butterworth-Heinemann, Oxford, ed. 5, 2011).

44. A. Ulvestad, A. Singer, J. N. Clark, H. M. Cho, J. W. Kim, R. Harder, J. Maser, Y. S. Meng, and O. G. Shpyrko, Topological defect dynamics in operando battery nanoparticles Science 2015, 348 (6241), 1344−1347.

45. Y. Zhou, and K. A. Fichthorn, Internal stress-induced orthorhombic phase in 5-fold-twinned noble metal nanowires. J. Phys. Chem. C, 2014, 118, 18746−18755.

46. Y. T. Zhu, X. Z. Liao, and R. Z. Valiev, Formation mechanism of fivefold deformation twins in nanocrystalline face-centered-cubic metals. Appl. Phys. Lett., 2005, 86, 103112.

47. S. Iijima, Fine particles of silicon, II. Decahedral multiply-twinned particles. Jpn. J. Appl. Phys. 1987, 26, 365-372.

48. V. Yamakov, D. Wolf, M. Salazar, S. R. Phillpot and H. Gleiter, Acta mater., 49, 2713; 2002c, ibid., 50, 61.

49. A. Ulvestad, A. Singer, H-M. Cho, J. N. Clark, R. Harder, J. Maser, Y. S. Meng, and O. G. Shpyrko, Single particle nanomechanics in operando batteries via lensless strain mapping. Nano Lett. 2014, 14, 5123–5127.

This journal is © The Royal Society of Chemistry 20xx

Please do not adjust margins